Real-Time Implementation of Different Controllers for a Two-wheeled Inverted Pendulum

Juan Villacrés, Michelle Viscaíno, Marco Herrera, Oscar Camacho

***Abstract*—**This paper presents experimental results of three control strategies to stabilize a two-wheeled inverted pendulum. The control techniques used are PID, Linear-Quadratic Regulator (LQR), and Sliding Mode Control. The comparison results of the three controllers are for angular wheel position tracking, for external disturbances, and parameter uncertainties in the model. Tests are quantified in terms of Integral Square Error – ISE. For the experiments, the robot was constructed with LEGO Mindstorms NXT 2.0.

***Keywords*—**LQR, PID, sliding mode control, robustness, tracking.

I. Introduction

The concept of a self-balancing a robot is based on the idea of the inverted pendulum model. An inverted pendulum is an open loop unstable system with highly nonlinear dynamics. The inverted pendulum problem is common in the field of control engineering. Therefore, it represents an ideal experiment for the design of classical and contemporary control techniques.

The type of robot used in this paper is a mobile robot with a two wheeled inverted pendulum, which is known as the Two-Wheeled Inverted Pendulum (TWIP) Robot NXT Lego Mindstorms. The robot has a body with two wheels for moving in a plane and whose head is similar to a human one. Two independent driving wheels are used for position control and for fast motion in a plane.

This work was supported by Escuela Politécnica Nacional.

Juan Villacrés is with the Departamento de Automatización y Control Industrial, Escuela Politécnica Nacional, Quito, Ecuador (e-mail: juan.villacres01@epn.edu.ec).

Michelle Viscaíno is with the Departamento de Automatización y Control Industrial, Escuela Politécnica Nacional, Quito, Ecuador (e-mail: michelle.viscaino@epn.edu.ec).

Marco Herrera, M.Sc. is with the Departamento. de Automatización y Control Industrial, Escuela Politécnica Nacional, Quito, Ecuador (e-mail: marco.herrera@epn.edu.ec).

Oscar Camacho, PhD. is with the Departamento de Automatización y Control Industrial, Escuela Politécnica Nacional, Quito, Ecuador and Facultad de Ingeniería, Universidad de los Andes, Mérida, Venezuela (e-mail: ocamacho@ula.ve).

The platform Lego Mindstorms NXT 2.0 is a kind of educational robotics which let us to assemble numerous mechanical configurations and besides allows the possibility of programming in various languages. Therefore, the uniqueness and wide application of technology derived from this unstable system has drawn interest of researchers and robotics enthusiasts around the world.

In the recent past, numerous scientists have been studying several control techniques in order to design stable mechanisms for this kind of systems. In [1], it is developed a study about a TWIP with JOE. The dynamics is derived using a Newtonian approach and then linearized around an equilibrium point for designing two decoupled state-space controllers. In [2], the dynamics of the TWIP mobile robot is studied using Kane's method of 3-DOF modeling, and the model is linearized to get a linear feedback control. In [3], two controllers for a wheeled inverted pendulum are designed. The first one is a two-level velocity controller for tracking vehicle orientation and heading speed set-points, while controlling the vehicle pitch (pendulum angle from the vertical) within a specified range. The second controller is also a two-level controller which stabilizes the vehicle's position to the desired point, while again keeping the pitch bounded between specified limits; however, the controller system designed is not robust with respect to parameter uncertainties. In [4], the model of the TWIP is derived and a full order sliding mode control is designed to control the robot, the results are obtained by simulations. In [5], a self-tuning PID control strategy, based on a model, is proposed for implementing a motion control system that stabilizes the two-wheeled vehicle and follows the desired motion commands. The controller parameters are tuned automatically, on-line, to overcome the disturbances and parameter variations. Experimental results are presented. In [6], a TWIP mobile robot is developed and the pole-placement state feedback controller is designed in order to verify the functionality of the robot. In [7] an adaptive fuzzy logic control of dynamic balance and motion is considered for wheeled inverted pendulums with parametric and functional uncertainties. In [8], a zero dynamics, derived by partial feedback linearization, is used to design a two degrees of freedom controller based on the feedforward controller and H∞ control technique to movement control of a TWIP. In [9], it is shown the design and development of a TWIP mobile robot using a Matlab® interfacing

configuration. The system is tested using a state-feedback controller. In [10], it is proposed a sliding mode control to solve a robust velocity tracking problem of mobile wheeled inverted pendulums models. In [11], a LQR and PID-PID are developed. Furthermore, the mathematical model is derived and the two controllers are compared, by simulations, in terms of input tracking and disturbances rejection capability. The results show that the LQR presents better performance than the PID controller. In [12] is designed and implemented a fuzzy control scheme for a TWIP using a Takagi-Sugeno fuzzy model. In [13], a sliding mode control and LQR are studied and compared. The SMC has the best performance by simulations. However, the work does not compare the controllers in terms of robustness.

In this study, three control techniques are used: a PID controller, a LQR, and a Sliding Mode control. They are designed and implemented for the TWIP. The paper includes both, simulations and real experimental results. The performance of the controllers, for this kind of unstable system with highly non-linear dynamic, is tested in terms of tracking and regulation.

The article begins with an introduction. Section II presents model of the robot that is used for controllers designing. Section III shows the development of the three controllers. Section IV presents the simulation results of TWIP with respect to body pitch angle and average angular position of wheels. Section V shows experimental results and the analysis of each controller respectively. Finally, the conclusions are presented in Section VI.

II. Dynamic Model

The TWIP used for this study has the following elements: NXT block, which is the brain of the robot; gyroscopic sensor, which measures the speed of inclination of the robot, $\dot{\psi}$, and allows to estimate the angle ψ; and two electric actuators (left and right wheels) with encoders, which measure the angular position of the wheel θ and estimate its speed $\dot{\theta}$.

The model was taken from [14] in which the equations are obtained by Lagrange method. The model is linearized around the operating point.

The model has four states and two inputs. The states are: the body pitch angle ψ $[rad]$, the average angular position of the wheels θ $[rad]$; and their respective velocities $\dot{\psi}$ $[rad/s]$ and $\dot{\theta}$ $[rad/s]$. The system inputs are the motor voltages u_l and u_r.

The robot system used is shown in Fig. 1

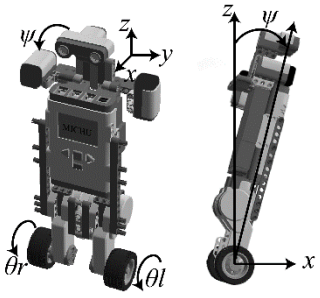

Fig. 1 System view: frontal, lateral and top.

The model is given by state-space representation:

$$\dot{x}_1 = A_1 x_1 + B_1 u\,. \tag{1}$$

Where:

$$x_1 = \begin{bmatrix} \theta \\ \psi \\ \dot{\theta} \\ \dot{\psi} \end{bmatrix}. \tag{2}$$

$$u = \begin{bmatrix} u_l \\ u_r \end{bmatrix}. \tag{3}$$

$$A_1 = \begin{bmatrix} 0 & 0 & 1 & 0 \\ 0 & 0 & 0 & 1 \\ 0 & a_{32} & a_{33} & a_{34} \\ 0 & a_{42} & a_{43} & a_{44} \end{bmatrix}. \tag{4}$$

$$B_1 = \begin{bmatrix} 0 & 0 \\ 0 & 0 \\ b_3 & b_3 \\ b_4 & b_4 \end{bmatrix}. \tag{5}$$

Where:

$$a_{32} = -gMLe_{12}/\det(E). \tag{6}$$

$$a_{42} = gMLe_{11}/\det(E). \tag{7}$$

$$a_{33} = -2(\sigma e_{22} + \beta e_{12})/\det(E). \tag{8}$$

$$a_{43} = 2(\sigma e_{12} + \beta e_{11})/\det(E). \tag{9}$$

$$a_{34} = 2\beta(e_{22} + e_{12})/\det(E). \tag{10}$$

$$a_{44} = -2\beta(e_{11} + e_{12})/\det(E). \tag{11}$$

$$b_3 = \alpha(e_{22} + e_{12})/\det(E). \tag{12}$$

$$b_4 = -\alpha(e_{11} + e_{12})/\det(E). \tag{13}$$

$$e_{11} = (2m + M)R^2 + 2J_w + 2n^2 J_m. \tag{14}$$

$$e_{12} = MLR - 2n^2 J_m. \tag{15}$$

$$e_{22} = ML^2 + J_\psi + 2n^2 J_m. \tag{16}$$

$$\det(E) = e_{11}e_{22} - e_{12}^2. \tag{17}$$

$$\alpha = nK_t/R_m. \tag{18}$$

$$\beta = nK_tK_b/R_m + f_m. \tag{19}$$

$$\sigma = \beta + f_w. \tag{20}$$

The physical parameters of TWIP are taken from [14] and some of them were modified according to our robot. In Table I these parameters are shown.

Table I. Parameters of TWIP

Parameter	Unit	Description
$g = 9.8$	$[m/s^2]$	Gravity acceleration
$m = 0.03$	$[kg]$	Wheel mass
$R = 0.021$	$[m]$	Wheel radius
$J_w = mR^2/2$	$[kg \cdot m^2]$	Wheel inertia moment
$M = 0.6$	$[kg]$	Body mass
$W = 0.09$	$[m]$	Body width
$D = 0.05$	$[m]$	Body depth
$H = 0.26$	$[m]$	Body height
$L = H/2$	$[m]$	Distance of the center of the mass from the Wheel axle
$J_\psi = ML^2/3$	$[kg \cdot m^2]$	Body pitch inertia moment
$J_\phi = M(W^2 + D^2)/12$	$[kg \cdot m^2]$	Body yaw inertia moment
$J_m = 1x10^{-5}$	$[kg \cdot m^2]$	DC motor inertia moment
$R_m = 6.69$	$[\Omega]$	DC motor resistance
$K_b = 0.468$	$[\mathrm{V \cdot s/rad}]$	DC motor back electromotive force constant
$K_t = 0.317$	[N. m/A]	DC motor torque constant
$n = 1$	Gear ratio	
$f_m = 0.0022$	Friction coefficient between body and DC motor	
$f_w = 0$	Friction coefficient between body and motion surface	

Replacing the physical parameter of the TWIP into equations (4) to (20). The matrices $A_1(t)$ and $B_1(t)$ are obtained:

$$A_1 = \begin{bmatrix} 0 & 0 & 1 & 0 \\ 0 & 0 & 0 & 1 \\ 0 & -698{,}30 & -416{,}80 & 416{,}80 \\ 0 & 139{,}96 & 53{,}41 & -53{,}41 \end{bmatrix}. \quad (21)$$

$$B_1 = \begin{bmatrix} 0 & 0 \\ 0 & 0 \\ 405{,}11 & 405{,}11 \\ -51{,}91 & -51{,}91 \end{bmatrix}. \quad (22)$$

Changing the continuous-time system into a discrete-time system with a sampling time of 10 [ms].

The following matrices are obtained:

$$A[k] = \begin{bmatrix} 1 & -0{,}010 & 0{,}003 & 0{,}007 \\ 0 & 1{,}004 & 0{,}0009 & 0{,}0091 \\ 0 & -1{,}122 & 0{,}1207 & 0{,}8690 \\ 0 & 0{,}649 & 0{,}1129 & 0{,}8910 \end{bmatrix}. \quad (23)$$

$$B[k] = \begin{bmatrix} 0{,}0068 & 0{,}0068 \\ -0{,}0009 & -0{,}0009 \\ 0{,}8546 & 0{,}8546 \\ -0{,}1097 & -0{,}1097 \end{bmatrix}. \quad (24)$$

The open-loop poles for the discrete-time system are:

$$p_1 = 1. \quad (25)$$

$$p_2 = 0{,}0091. \quad (26)$$

$$p_3 = 1{,}0703. \quad (27)$$

$$p_4 = 0{,}9362. \quad (28)$$

As it is shown in equations from (25) to (27) the system is open-loop unstable, since it has two poles over or outside the unit circle.

III. Controllers Synthesis

In this section the synthesis of each one of the three controllers, to stabilize the TWIP, is presented. Firstly, the PID is presented, then the LQR and finally the SMC is described.

A. PID

PID is the most common controller used in industrial control systems [11]. In order to implement a PID controller, the continuous PID (29) must be discretized. The trapezoidal integration is used to integral component and for the derivative component the forward integration is used, the equation is given as in (30), [15].

$$G_c = K_P + K_D s + \frac{K_I}{s}. \quad (29)$$

$$\frac{U(z)}{E(z)} = K_P + K_I\left(\frac{T_0}{2}\frac{z+1}{z-1}\right) + K_D\left(\frac{1}{T_0}\frac{z-1}{z}\right). \quad (30)$$

Taking the inverse Z transform (31) of (30), (32) is obtained.

$$z^{-n}F(z) = F(k-n). \quad (31)$$

$$\begin{aligned} u(k) = u(k-1) + E(k)\left(K_P + \frac{K_I T_0}{2} + \frac{K_D}{T_0}\right) \\ + E(k-1)\left(-K_P + \frac{K_I T_0}{2} \right. \\ \left. - \frac{2K_D}{T_0}\right) + E(k-2)\left(\frac{K_D}{T_0}\right). \end{aligned} \quad (32)$$

And:

$$E(k) = x_{ref}\ (k) - x(k). \quad (33)$$

Where:

x_{ref}: It represents the desired states, in order to stabilize the TWIP. $x_{ref} = 0$

x: It represents the value of the system outputs.

Two PID controllers are designed, Fig. 2 shows the scheme. The first PID controller is designed in order to control the body pitch angle and the second PID to regulate the angular

position of the wheels.

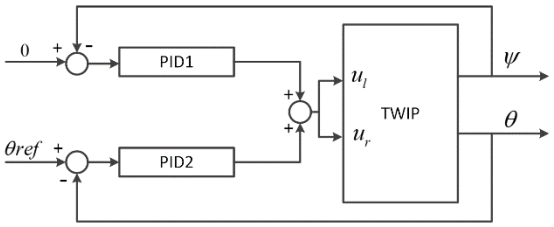

Fig. 2 PID Controller Scheme.

In Table II the tuning parameters for PID controllers, which are obtained by trial and error, are shown.

Table II. PID parameters

	Variable	K_P	K_I	K_D
PID1	ψ	-77.97	-0.01	-8.79
PID2	θ	-1.07	-0.01	-1.36

B. LQR

The Linear Quadratic Regulator is a state-feedback control, which is useful to handle multivariable systems. The aim of LQR is to minimize a cost function, [15]. The control scheme is shown in Fig. 3.

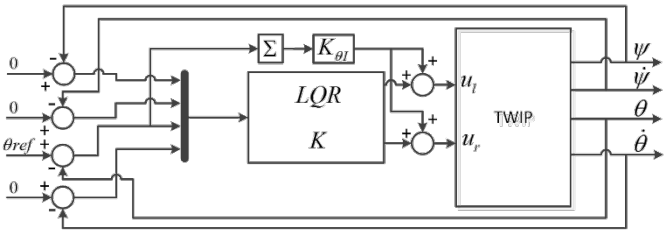

Fig. 3 LQR Scheme.

The system is given by the following equation:

$$x(k+1) = Ax(k) + Bu(k). \tag{34}$$

The optimal control will be written as a state feedback, given by the next expression:

$$u(k) = -Kx(k). \tag{35}$$

Where:

K is the gain matrix. The matrix K has to bring the system into a final state $x(k_1) = 0$ from an initial state $x(k_0)$.

To determine the matrix K the performance index, J, also called the cost function, should be minimized.

$$J = \sum_{k=k_0}^{k_1-1} x^T(k+1)Qx(k+1) + u^T(k)Ru(k). \tag{36}$$

Selecting the matrices Q (37) and R (38), as follow:

$$Q = \begin{bmatrix} 0{,}38 & 0 & 0 & 0 \\ 0 & 0{,}43 & 0 & 0 \\ 0 & 0 & 0{,}09 & 0 \\ 0 & 0 & 0 & 0{,}09 \end{bmatrix}. \tag{37}$$

$$R = \begin{bmatrix} 0{,}00017 & 0 \\ 0 & 0{,}00017 \end{bmatrix}. \tag{38}$$

Solving the equation (36). The matrix K (39) is obtained:

$$K = \begin{bmatrix} -1{,}099 & -81{,}44 & -1{,}368 & -10{,}860 \\ -1{,}099 & -81{,}44 & -1{,}368 & -10{,}860 \end{bmatrix}. \tag{39}$$

An integral term is added to eliminate the position error. Therefore, the control law is:

$$\begin{bmatrix} u_l \\ u_r \end{bmatrix} = -Kx(k) + \begin{bmatrix} K_{\theta I} \sum \left(\theta_{ref}(k) - \theta(k)\right) \\ K_{\theta I} \sum \left(\theta_{ref}(k) - \theta(k)\right) \end{bmatrix}. \tag{40}$$

Where:

$K_{\theta I}$: It represents an integral constant and $K_{\theta I} = -0{,}006$

C. Sliding Mode Control

Sliding Mode control (SMC) is a kind of robust control, [10, 16]. The control scheme is shown in Fig. 4.

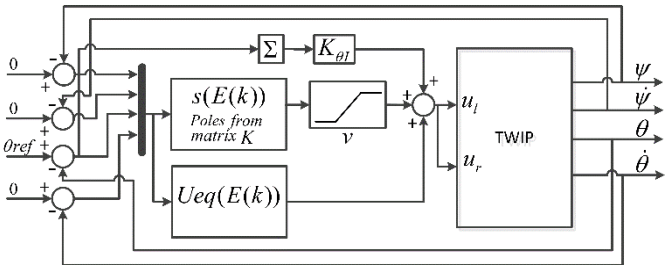

Fig. 4 SMC Scheme.

From equation (34) and using the transformation matrix T_1, [15]. The system is transformed into its controllable canonical form (41)

$$\bar{x}(k+1) = \bar{A}\bar{x}(k) + \bar{B}u(k). \tag{41}$$

Where:

$$\bar{A} = T_1^{-1}AT_1. \tag{42}$$

$$\bar{B} = T_1^{-1}B. \tag{43}$$

The sliding surface is defined as:

$$s\big(x(k)\big) = Sx(k) = \bar{S}\bar{x}(k) \quad \bar{S} \in \mathbb{R}^{1xn}. \tag{44}$$

Where:

$$\bar{S} = ST_1. \tag{45}$$

$$\bar{S} = [\bar{s_1} \quad \bar{s_2} \ldots \overline{s_{n-1}} \quad 1]. \tag{46}$$

Thereby, the sliding surface is defined as in (47).

$$s\big(x(k)\big) = \bar{S}\bar{x}(k) = 0. \tag{47}$$

$$\bar{S}\bar{x}(k) = \bar{s_1}y + \bar{s_2}y^k + \cdots + \overline{s_{n-1}}y^{k(n-2)} + y^{k(n-1)}. \tag{48}$$

$$Sx(k+1) = 0. \tag{49}$$

$$Sx(k+1) = S\left(Ax(k) + Bu_{eq}(k)\right) = 0. \tag{50}$$

Therefore, from the equivalent control procedure:

$$u_{eq}(k) = -(SB)^{-1}SAx(k). \tag{51}$$

The complete SMC, Eq. (52), is composed by a continuous part, (51), and discontinuous part, (53), and can be represented as:

$$u(k) = u_{eq}(k) + v. \tag{52}$$

$$v = \begin{cases} cte, & s(x) < 0 \\ 0, & s(x) = 0. \\ -cte, & s(x) > 0 \end{cases} \tag{53}$$

In order to perform the angular wheel position tracking, the sliding surface and equivalent control depend on the error (33) instead of the state.

The sliding surface is designed with the poles obtained from feedback the matrix K (39). The sliding surface takes into account the optimal poles obtained from the LQR and therefore produces the best possible sliding movement until get the final desired value.

$$s\big(E(k)\big) = [1{,}924 \quad 147{,}918 \quad 1{,}669 \quad 21{,}065]. \tag{54}$$

And the equivalent control law is:

$$u_{eq}(E(k)) = [-1{,}924 \quad -160{,}270 \quad -2{,}717 \quad -21{,}581]. \tag{55}$$

In order to reduce the chattering produced by high frequency switching, a filter is used (56), where $cte = 0{,}3$ and $L = 0{,}64$.

$$v = \begin{cases} -cte, & s\big(E(k)\big) < -L \\ \dfrac{s}{L}, & \left|s\big(E(k)\big)\right| \le L. \\ cte, & s\big(E(k)\big) > L \end{cases} \tag{56}$$

The filter is shown in Fig. 5.

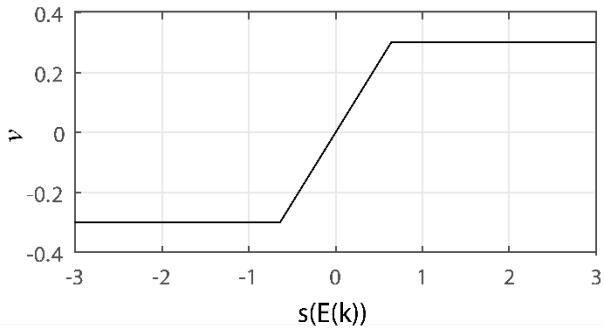

Fig. 5 Filter for chattering reduction.

An integral part is aggregated by maintaining the error position equal to zero. Thus, the control law is given by the following expression:

$$u_l = u_r = u_{eq}(k) + v + K_{\theta I}\sum(\theta_{ref}(k) - \theta(k)). \tag{57}$$

Where:

$K_{\theta I}$: It represents an integral constant and $K_{\theta I} = -0{,}006$.

IV. Simulation Results

In this section, the simulation results are presented using Simulink-Matlab®. The performance of the controllers is tested with an initial condition in the body pitch angle.

$$x_0 = [0 \quad 0{,}1 \quad 0 \quad 0]^T. \tag{58}$$

Figures 6, 7, and 8 show the evolution of the Body Pitch Angle ψ, Angular Wheel Position θ and input to the system u.

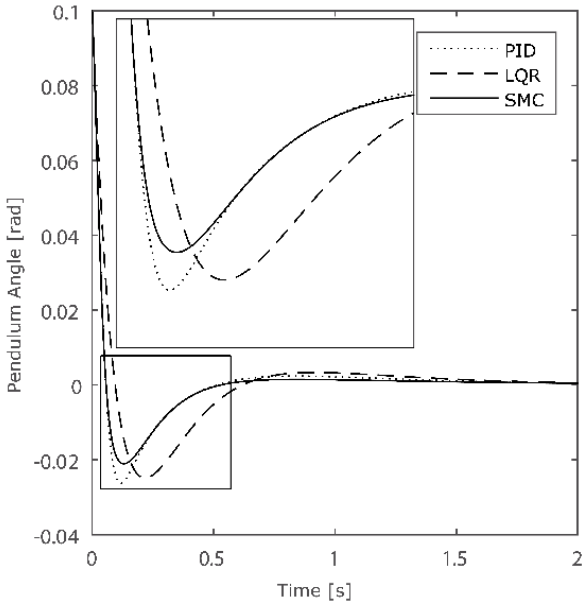

Fig. 6 Body pitch angle.

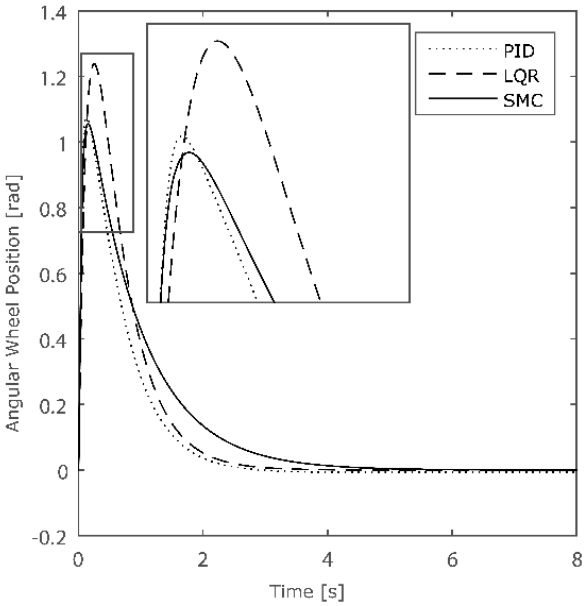

Fig. 7 Angular wheel position.

The Sliding Mode Control presents the best response to stabilize the TWIP. It has a smooth response and the smallest overshoot in ψ and θ. The output of the Sliding Mode Controller does not present chattering, it can be seen in Figure 8.

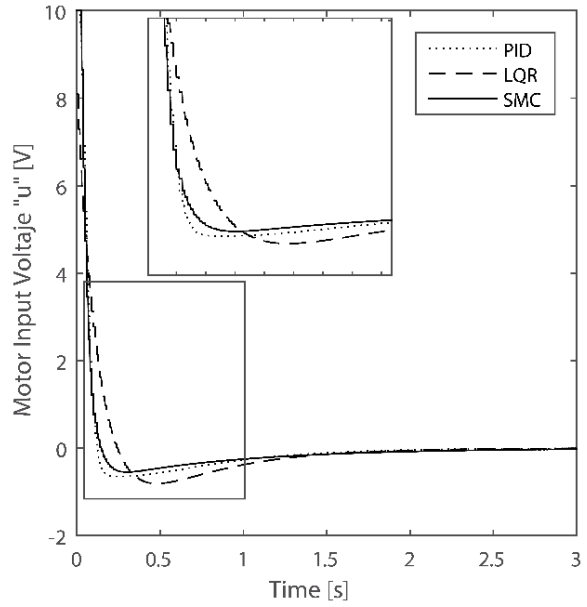

Fig. 8 Motor input voltage

V. Experimental Results

In this section, the experimental results are shown. All the controllers are implemented and applied to the educational platform Mindstorms NXT 2.0, of Lego, in the TWIP configuration.

In order to compare the performance of the controllers in real-time, three tests are carried out. The test considered are: disturbances case, robustness to model uncertainties and disturbances, and the last test considers tracking and disturbances over a steep path.

All controllers, in the three test, are compared using the Integral Square Error (ISE). The ISE is calculated with:

$$ISE = \int_0^t \big(e(t)\big)^2 dt. \quad (57)$$

Where:

$e(t)$: It represents the error between the reference and the state feedback.

A. Disturbance

For this test, an external force F is used. The force is exerted using a pendulum system as it is shown in Fig. 9.

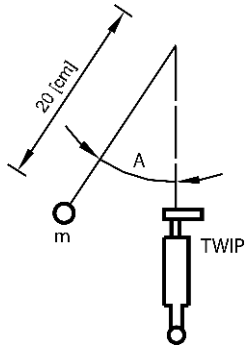

Fig. 9 Scheme used to apply an external force

The force is obtained by:

$$F = m \cdot g \cdot \sin(A). \quad (58)$$

Where:

m: It represents the mass of the pendulum system; its value is 0.03 $[kg]$.

g: It represents the gravity, the value is 9.8 $[m/s^2]$.

A: It is the angle formed between the vertical axis and the rope holding the mass. In this case, the angle is 35°.

Solving the equation (58). The resulting force F (59) is:

$$F = 0{,}1686\ (N \cdot m). \quad (59)$$

Fig. 10 shows the test evolution, in the first picture the TWIP is stabilized, then in the second picture the force F is applied to the TWIP, in pictures 3 and 4 the TWIP tries to stabilize and finally picture 5 show the TWIP stable.

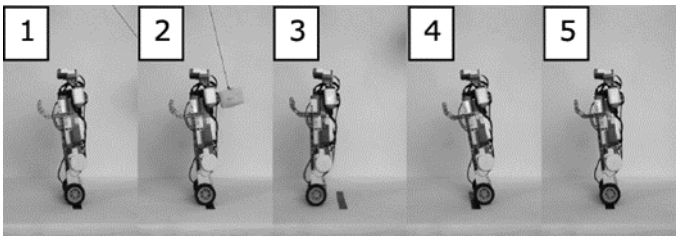

Fig. 10 Test evolution when an external force is applied.

As is shown in Figures 11, 12, and 13 the progression of the Body Pitch Angle ψ, Angular Wheel Position θ and input to the system u are pictured for each controller.

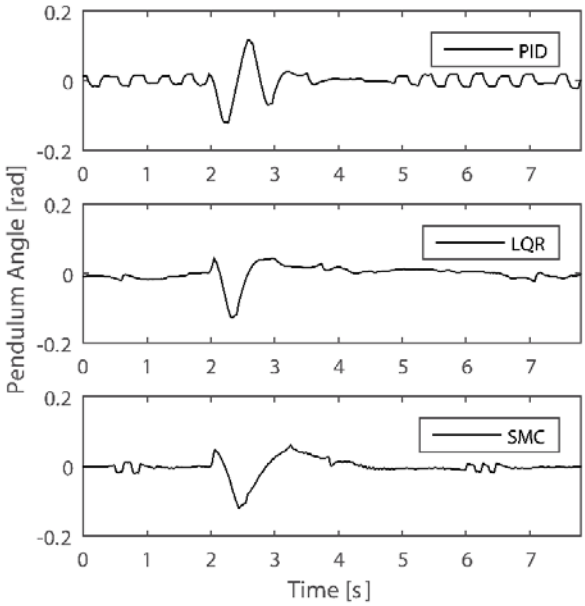

Fig. 11 Body pitch angle.

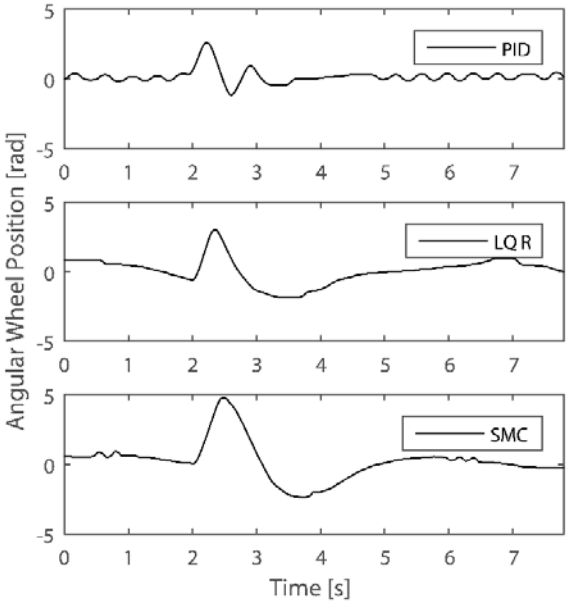

Fig. 12 Angular wheel position.

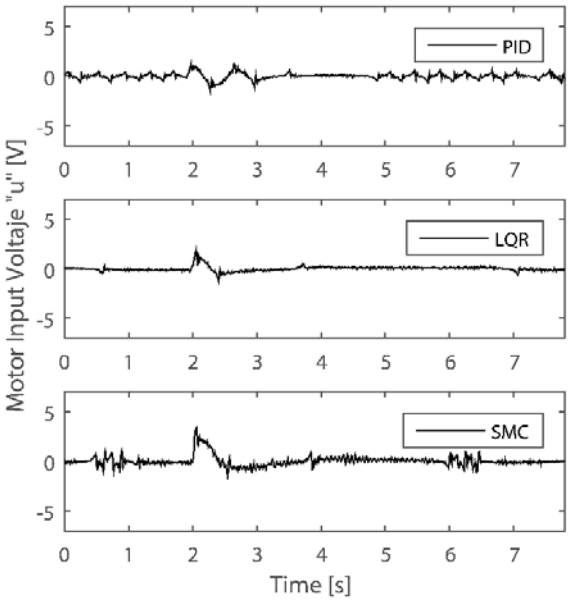

Fig. 13 Motor input voltage.

Table III. ISE Comparison of three controllers with disturbance.

	PID	LQR	SMC
	ISE		
ψ	0.0066	0.0047	0.0051
θ	2.2081	7.0679	15.3873

The LQR presents the best response, with less overshoot and less oscillations. The LQR output is smoother and with a lower settling time.

B. Model uncertainties

Fig. 14 illustrates this test. Firstly, the robot weight is increased in 40%, it can be observed in picture 1. Picture 2 shows that the robot is hit with an external force of $0{,}147\ (Nm)$ with an angle equal to 30°, in the next two figures the robot tries to stabilize.

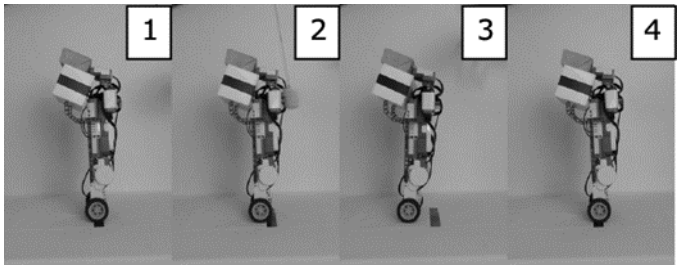

Fig. 14 Increasing the weight and external force.

Figures 15, 16, and 17 show the evolution of the Body Pitch Angle ψ, Angular Wheel Position θ and input to the system u.

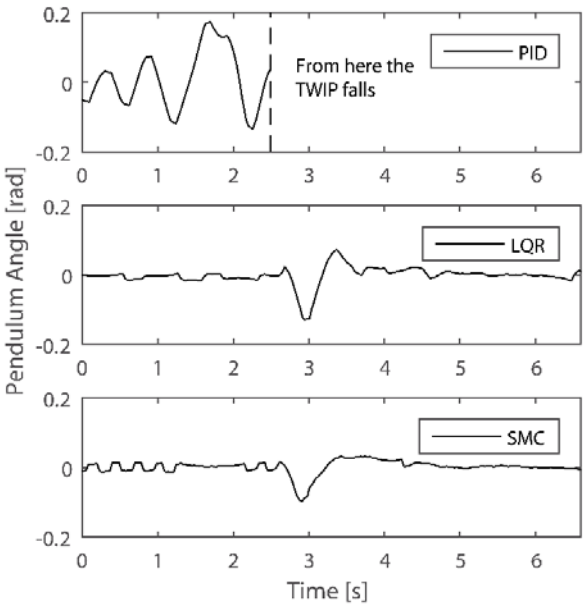

Fig. 15 Body pitch angle.

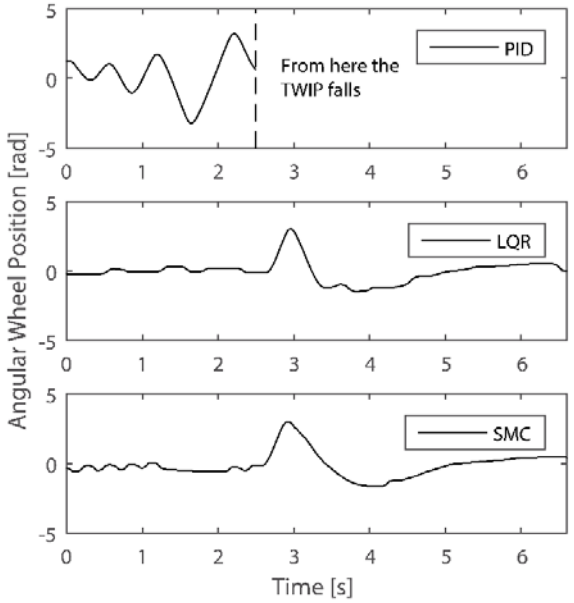

Fig. 16 Angular wheel position.

Table IV. ISE Comparison of three controllers with model uncertainties

	PID	LQR	SMC
	ISE		
ψ	0.0175	0.0045	0.0027
θ	6.1256	4.2191	5.4097

In this test, The PID controller was not able to stabilize the TWIP as is shown in Fig. 15. For this reason any force was applied over the TWIP. LQR and SMC responses are very close.

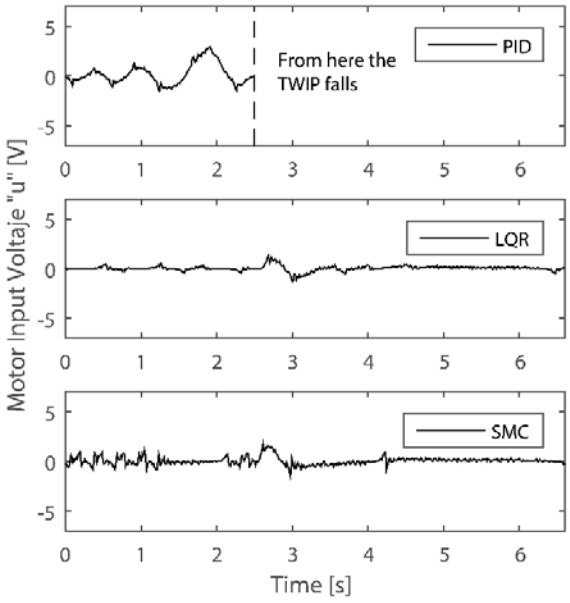

Fig. 17 Motor input voltage.

C. *Tracking and disturbances*

In the third test, a steep path is used as reference. The surface pattern used is shown in Fig. 18. It has a downward ramp and a step to simulate disturbances.

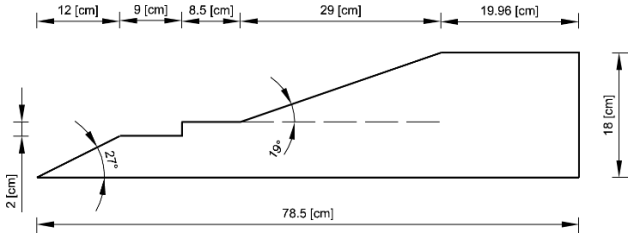

Fig. 18 Surface scheme for tracking and disturbances test.

Fig. 19 shows the progress of the robot on the steep path. It can be seen from picture 1 to figure 9.

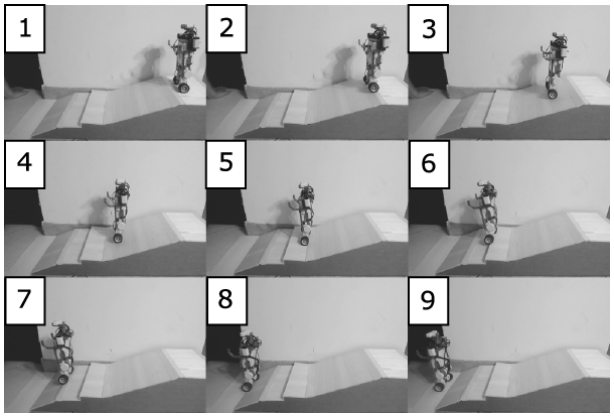

Fig. 19 TWIP tracking over a steep path

Figure 20 shows how the TWIP maintains upright in spite of the unevenness of the surface. The tracking results are shown in Fig. 21.

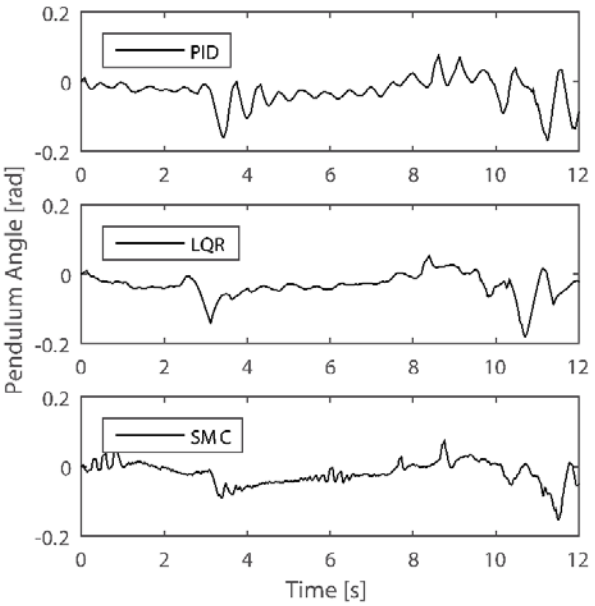

Fig. 20 Body pitch angle

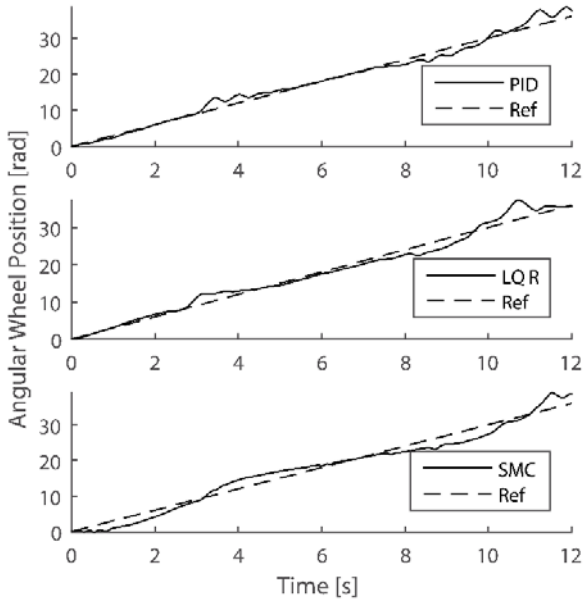

Fig. 21 Angular wheel position.

Table V. ISE Comparison of three controllers in terms of tracking and disturbance.

	PID	LQR	SMC
	ISE		
ψ	0.0168	0.0159	0.0107
θ	10.7178	13.6665	32.8634

SMC offers the best response to control the TWIP pitch angle, but PID and LQR present better results than SMC to control the angular position of wheels.

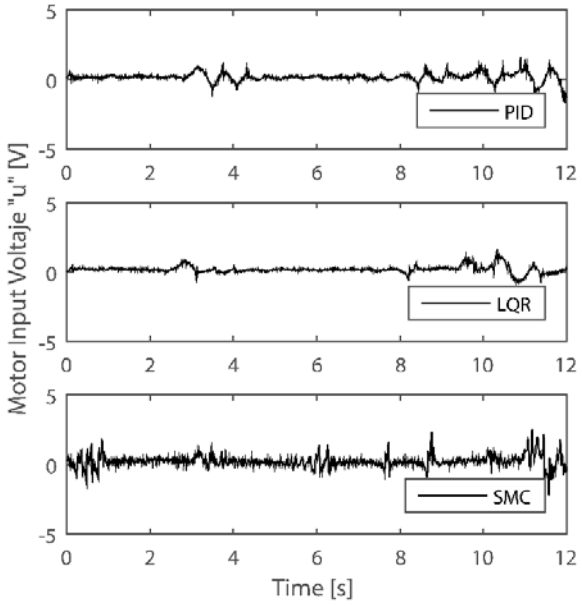

Fig. 22 Motor input voltage.

VI. Conclusions

In this article, three controllers: PID, LQR, and Sliding Mode Controller (SMC) were successfully designed and implemented to stabilize a TWIP.

Based on the results, for nominal cases, on both simulation and experimental results, it can be concluded that the three implemented control schemes are capable to stabilize the TWIP.

All the controllers were compared. The SMC had a better performance than LQR and PID for the body pith angle. The LQR response was faster than the other two. The SMC had a better disturbance rejection capability than LQR and PID controllers. In the real experiments the SMC output presents a little chattering in spite of the filter, which is not presented in the simulation results.

For modeling uncertainty case, the Sliding Mode Controller showed better response than the other two. The PID fails in the second test.

Finally, three controllers were able to control the TWIP when a steep pattern is used.

Acknowledgment

Oscar Camacho thanks to PROMETEO project of SENESCYT. Republic of Ecuador, for its sponsorship in the realization of this work.

REFERENCES

[1] Grasser, F., D'arrigo, A., Colombi, S., & Rufer, A. C. "JOE: a mobile, inverted pendulum." Industrial Electronics, *IEEE Transactions* on 49.1 (2002): pp. 107-114.

[2] Kim, Yeonhoon, Soo Hyun Kim, and Yoon Keun Kwak. "Dynamic analysis of a nonholonomic two-wheeled inverted pendulum robot." *Journal of Intelligent and Robotic Systems* 44.1 (2005): pp. 25-46.

[3] Pathak, Kaustubh, Jaume Franch, and Sunil K. Agrawal. "Velocity and position control of a wheeled inverted pendulum by partial feedback linearization."Robotics, *IEEE Transactions* on 21.3 (2005): pp. 505-513.

[4] Nawawi, S. W., M. N. Ahmad, and J. H. S. Osman. "Control of two-wheels inverted pendulum mobile robot using full order sliding mode control." *Proceedings of International Conference on Man-Machine Systems*. 2006.

[5] Ren, Tsai-Jiun, Tien-Chi Chen, and Chun-Jung Chen. "Motion control for a two-wheeled vehicle using a self-tuning PID controller." *Control Engineering Practice* 16.3 (2008): pp. 365-375.

[6] Nawawi, Sophan Wahyudi, Mohamad Noh Ahmad, and Johari Halim Shah Osman. "Development of a two-wheeled inverted pendulum mobile robot."Research and Development, 2007. SCOReD 2007. *5th Student Conference on. IEEE*, 2007.

[7] Li, Zhijun, and Chunquan Xu. "Adaptive fuzzy logic control of dynamic balance and motion for wheeled inverted pendulums." Fuzzy Sets and Systems 160.12 (2009): pp. 1787-1803.

[8] Shimada, Akira, and Naoya Hatakeyama. "Movement control of two-wheeled inverted pendulum robots considering robustness." *SICE Annual Conference, 2008. IEEE*, 2008.

[9] Nawawi, S. W., M. N. Ahmad, and J. H. S. Osman. "Real-time control of a two-wheeled inverted pendulum mobile robot." *World Academy of Science, Engineering and Technology* 39 (2008): pp. 214-220.

[10] Huang, Jian, et al. "Robust velocity sliding mode control of mobile wheeled inverted pendulum systems." *Robotics and Automation, 2009. ICRA'09. IEEE International Conference on. IEEE*, 2009.

[11] Nasir, A. N. K., M. A. Ahmad, and RMT Raja Ismail. "The control of a highly nonlinear two-wheels balancing robot: A comparative assessment between LQR and PID-PID control schemes." *World Academy of Science, Engineering and Technology 70* (2010): pp. 227-232.

[12] Huang, Cheng-Hao, Wen-June Wang, and Chih-Hui Chiu. "Design and implementation of fuzzy control on a two-wheel inverted pendulum." *IEEE Transactions on Industrial Electronics* (2011). 58(7), pp. 2988-3001.

[13] Torchani, Borhen, et al. "Comparative analysis of the saturated sliding mode and LQR controllers applied to an inverted pendulum." *Communications, Computing and Control Applications (CCCA), 2011 International Conference on. IEEE*, 2011.

[14] Gu, D. W., P. Petkov, and M. M. Konstantinov. "Robust control design with MATLAB, Advanced Textbooks in Control and Signal Processing." (2013).

[15] Villacrés, J., Viscaíno, M., Herrera, M. and Camacho, O. "Controllers Comparison to stabilize a Two-wheeled Inverted Pendulum: PID, LQR and Sliding Mode Control." *International Journal of Control Systems and Robotics* (2016): pp. 29-36.

[16] Rojas R., Camacho O. and González L. "A sliding mode control proposal for open-loop unstable processes" *ISA transactions* (2004). 43 (2), pp. 243-255.

Juan Villacrés was born in Quito, Ecuador, on July 9th, 1992. He received the Bachelor in Electronical and Automation Engineering from Escuela Politécnica Nacional (EPN), Quito, Ecuador. He is a Research Assistant and his research interests include robotics, control in real-time, path-planning, systems and control theory.

Michelle Viscaíno was born in Quito, Ecuador, on May 6th, 1992. She received the Bachelor in Electronical and Automation Engineering from Escuela Politécnica Nacional (EPN), Quito, Ecuador. She is a Research Assistant at EPN and her current research interests include robotics, control systems and artificial vision.

Marco Herrera received B.Sc. degree in Electronics and Control Engineering from Escuela Politécnica Nacional (EPN), Quito, Ecuador, in 2009. He received M.Sc. degree in Automation and Robotics from Universidad Politécnica de Madrid (UPM), Spain, in 2014. From 2010 – 2012, he was Assistan Professor at Universidad Internacional del Ecuador, Quito, Ecuador. Since 2014 he is Assistant Professor at Departamento de Automatización y Control Industrial at Escuela Politécnica Nacional. His main teaching and research activities have been related to the Control System and Robotics. His research interest include optimal control, sliding mode control and fuzzy modelling and control applications.

Oscar Camacho received the Bachelor in Electrical Engineer from Universidad de los Andes (ULA), Mèrida, Venezuela in 1984. He received the MSc. Control Engineering ULA in 1992 (ULA), 1992. He moved to the University of South Florida, Tampa (USF), Florida in United States 1992. In 1994 he got a ME in Chemical Engineering and in 1996 a PhD, both at USF. Postdoctoral Development activities at USF in 2001. He has held teaching and research in the ULA and PDVSA (Venezuela), USF (USA) and EPN (Ecuador). He was Director of the School of Electrical Engineering Coordinator of the Master Program in Automation and Instrumentation, Dean of the Engineering Faculty at ULA, from 2005 until 2014. He is Associated Editor of the Journal ISA Transactions. Reviewer in different scientific journals. His current research interests include sliding mode control process control systems with long delay, chemical process control. He has authored more than 100 publications in journals and conference proceedings.